Dalton Transactions

PAPER

Aryl-NHC-group 13 trimethyl complexes: structural, stability and bonding insights†

Melissa M. Wu,[a] Arran M. Gill,[b] Lu Yunpeng,[a] Li Yongxin,[a] Rakesh Ganguly,[a] Laura Falivene*[c] and Felipe García*[a]

Treatment of aromatic N-substituted N-heterocyclic carbenes (NHCs) with trimethyl-gallium and -indium yielded the new Lewis acid–base adducts, IMes·GaMe$_3$ (1), SIMes·GaMe$_3$ (2), IPr·GaMe$_3$ (3), SIPr·GaMe$_3$ (4), IMes·InMe$_3$ (5), SIMes·InMe$_3$ (6), IPr·InMe$_3$ (7), and SIPr·InMe$_3$ (8), with all complexes being identified by X-ray diffraction, IR, and multinuclear NMR analyses. Complex stability was found to be largely dependent on the nature of the constituent NHC ligands. Percent buried volume (%V_{Bur}) and topographic steric map analyses were employed to quantify and elucidate the observed trends. Additionally, a detailed bond snapping energy (BSE) decomposition analysis focusing on both steric and orbital interactions of the M–NHC bond (M = Al, Ga and In) has been performed.
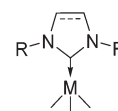
Introduction

Over the past thirty years, the use of Arduengo carbenes to stabilize transition metal compounds for organic syntheses has been intensively studied.[1,2] Conversely, in the case of N-heterocyclic carbene group 13 metal complexes,[3] only a limited range of compounds have been applied to organic transformations,[3b,4] despite having shown excellent catalytic activity in ring opening polymerization reactions (ROPs).[4a,c] Previous studies have shown that slight modifications within these complexes can result in drastic changes in their reactivity towards organic transformations – a good example of this being the greater product yields and selectivity displayed by IMes·AlH$_2$Cl over IMes·AlHCl$_2$ in hydroalumination reactions on carbonyl or epoxide containing substrates.[3b] Cole et al. have attributed this observation to a stronger Al–H bond and increased steric bulk in IMes·AlHCl$_2$ resulting in poorer catalytic activity. Reports by Hevia et al.[5a] on the structure, stability and isomerization reactions between normal (n) and abnormal (a) NHC–gallium alkyl complexes further highlight the importance of steric and electronic factors in the stability and accessibility of both normal and abnormal NHC main group com-

plexes. Whilst Dagorne et al.[5b] described the normal-to-abnormal NHC rearrangement and small molecule activation on the aluminium, gallium and indium triad. With much yet to be explored, the synthesis, characterization, and reactivity of new NHC group 13 complexes remain an exciting area for the main group and organic chemists alike. Our group has previously reported that minimal adjustment to the steric properties of the constituent NHC moiety in trimethylaluminium complexes can have a profound effect on their stability (Fig. 1, A–D). This prompted us to seek to quantify and rationalize the structure–stability–reactivity relationships of heavier group 13 NHC counterparts, using the commonly employed IMes, SIMes, IPr and SIPr carbenes as case studies.

Herein, we firstly report the synthesis and characterization of a series of aromatic N-substituted NHC gallium and indium alkyl complexes. By combining X-ray crystallographic and spectroscopic studies with theoretical calculations, we then assess the stability and bonding characteristics of these complexes.

[a]School of Physical and Mathematical Sciences, Division of Chemistry and Biological Chemistry, Nanyang Technological University, 21 Nanyang Link, Singapore, 637371, Singapore. E-mail: Fgarcia@ntu.edu.sg; Fax: (+65)67911961
[b]Chemistry, Faculty of Natural and Environmental Sciences, University of Southampton, Highfield Southampton, SO17 1BJ, UK
[c]King Abdullah University of Science and Technology, Building 9, Level 4, Room #4358, Thuwal, 23955-6900, Saudi Arabia. E-mail: laura.falivene@kaust.edu.sa

Fig. 1 New NHC trimethyl-gallium, -indium, and -aluminium complexes. IMes·GaMe$_3$ (1), SIMes·GaMe$_3$ (2), IPr·GaMe$_3$ (3), SIPr·GaMe$_3$ (4), IMes·InMe$_3$ (5), SIMes·InMe$_3$ (6), IPr·InMe$_3$ (7), SIPr·InMe$_3$ (8), IMes·AlMe$_3$ (A), SIMes·AlMe$_3$ (B), IPr·AlMe$_3$ (C), and SIPr·AlMe$_3$ (D).[6b]

An insightful comparison between group 13-NHC complexes with transition metal–NHC and –PHC (using Al–IMes, Pd–IMes and Pd(P)–IMes as case studies) is also provided.

Results and discussion

Synthesis of complexes 1–8

The general synthetic route for the synthesis of these complexes is *via* the formation of Lewis acid–base adducts (Scheme 1).[4–7] Hence, treatment of 1 equivalent of carbene (IMes, SIMes, IPr and SIPr) with trimethylgallium[8] or indium[9] resulted in the formation of their respective complexes IMes·GaMe₃ (**1**), SIMes·GaMe₃ (**2**), IPr·GaMe₃ (**3**), SIPr·GaMe₃ (**4**), IMes·InMe₃ (**5**), SIMes·InMe₃ (**6**), IPr·InMe₃ (**7**), and SIPr·InMe₃ (**8**) as shown in Fig. 1. Isolation of compounds was performed by crystallization in ether or toluene at room temperature or at 0 °C.[9]
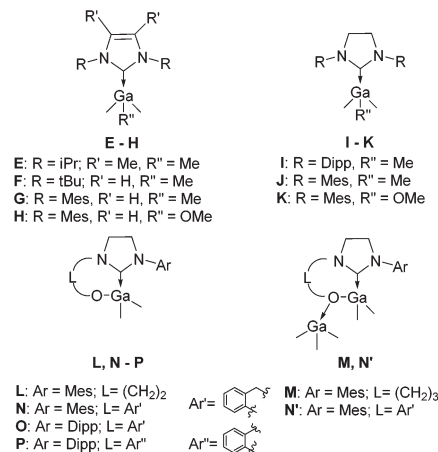
All compounds are highly air- and moisture-sensitive and traces of decomposition were consistently observed during their characterization. Hence, all attempts of elemental analyses were unsuccessful. Moreover, this was also observed for **4** and **8** in the solid state, where argon-gas-stored samples slowly decomposed at room temperature.

Crystallographic studies of complexes 1–8

Complexes **2**–**6** recrystallized from solution as two crystallographically independent, but chemically equivalent, molecules and only one molecule will be described herein. Complexes **6** and **8** are the first structurally characterized trimethylindium complexes containing saturated NHC moieties. Previously reported gallium and indium NHC species are, for the most part, heteroleptic complexes (see Fig. 2 and 3). Furthermore, only four trimethylgallium complexes have been previously structurally characterized (*i.e.*, **E**,[4f] **G**,[4a] **I**[4a] and **J**,[4c] see Fig. 2).[3,4,10] Generally, heavy group 13 NHC complexes adopt a four coordinate, distorted tetrahedral geometry at the metal centre, with the exception of indium complexes **R**, **S** and **T** (IMes·InMe₂Cl, IMes·InMe₂OTf and IMes·InMe(OTf)₂, respectively).[4d] Despite being four-coordinate, the indium centre of complex **R** does not conform to a distorted tetrahedral geometry due to the weak carbene chloride interaction
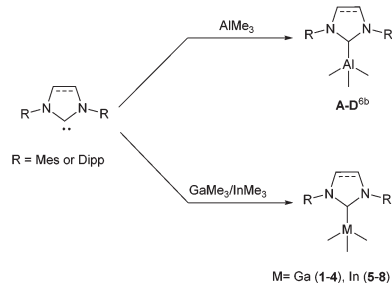
Fig. 2 Previously reported trimethyl and dimethylgallium complexes **E**,[4f] **F**,[5b] **G**–**I**,[4a] and **J**–**P**.[4b,b]
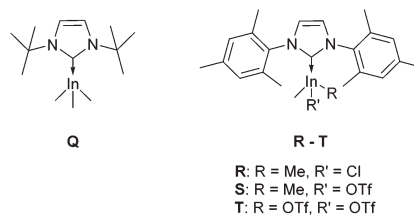
Fig. 3 Previously reported mono-, di- and trimethylindium complexes **Q**[5b] and **R**–**T**.[4d]

that causes the chloride to lie orthogonal to the carbene plane.[4d] In the case of complexes **S** and **T**, the indium centres interact with an additional neighbouring triflate substituent belonging to an adjacent molecule, hence directing the complex geometry towards a pentacoordinate trigonal bipyramidal geometry in the solid state.[4d]

The molecular structures of compounds **1**–**8** revealed the formation of four-carbon-coordinated gallium and indium atoms attached to three alkyl groups, and the presence of a neutral carbene moiety (see Fig. 4 and 5). The distorted tetrahedral geometry at the gallium and indium centres is evidenced by the C–M–C bond angles that range from 100.0° to 115.3° and 99.6° to 119.1° for gallium and indium, respectively, with metal to carbene carbon (M–C$_{carbene}$) bond lengths ranging from 2.111 Å to 2.137 Å, and 2.301 Å to 2.342 Å for gallium and indium, respectively. In the case of **1**–**4**, the Ga–C$_{carbene}$ bond lengths are consistent with the previously reported trimethylgallium complexes (*cf.* 2.130(2) Å, 2.105(2) Å, 2.132(3) Å and 2.121(3) Å and for **E**, **G**, **I**, and **J**, respectively) (see Table 1).[4a,e,f] In agreement with our previous observations for the lighter trimethylaluminium counterparts, similar M–C$_{carbene}$ bond distances between SIPr·AlMe₃ and the less sterically encumbered IiPrMe·AlMe₃ (2.127(2) Å and 2.124(6) Å, respectively)[4f,6b,11,12] were observed. The Ga–C$_{carbene}$ bond distance in **4** is also comparable to that of IiPrMe·GaMe₃ (**E**) (2.137(2) Å and 2.130(2) Å, respectively).[4f]

Scheme 1 Synthetic strategy for the NHC adducts. Mes (2,4,6-trimethylphenyl); Dipp (2,6-diisopropylphenyl).

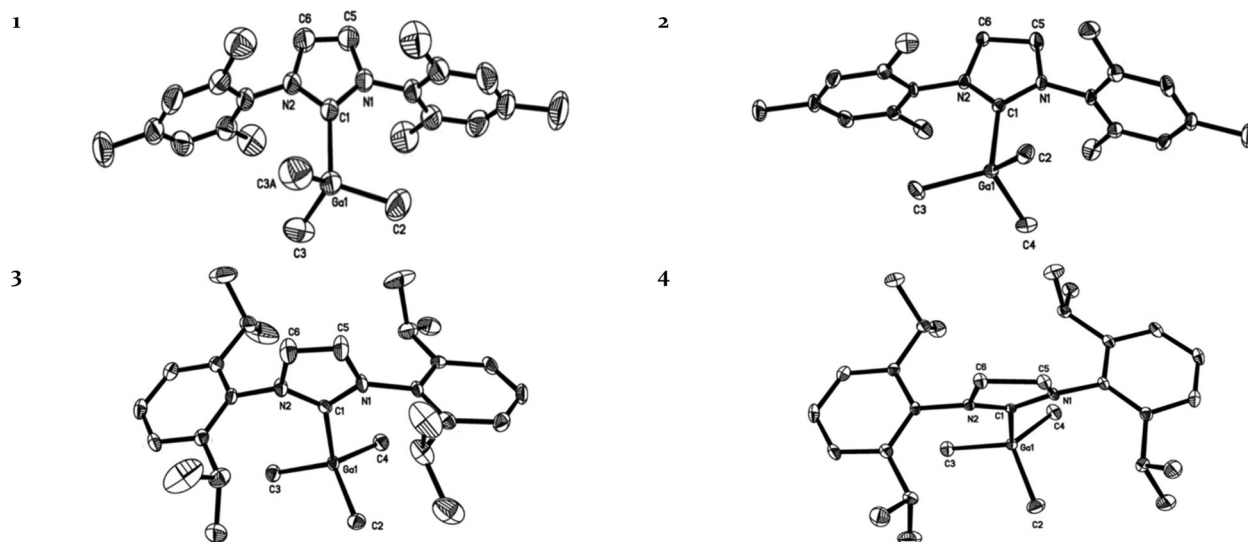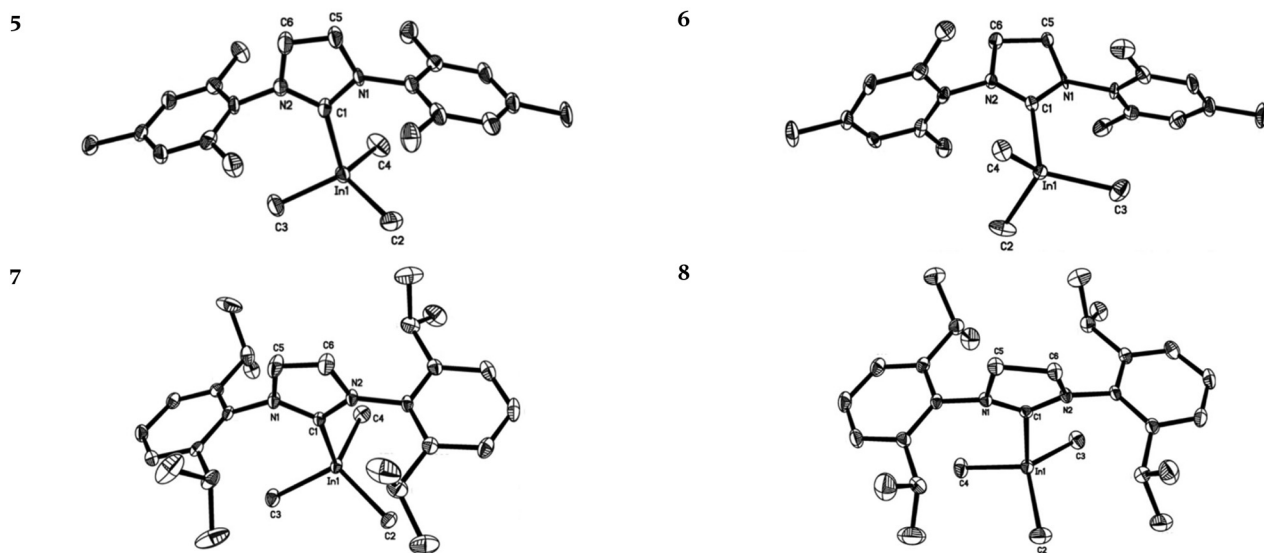**Fig. 4** Molecular structures of IMes·GaMe$_3$ (**1**), SIMes·GaMe$_3$ (**2**), IPr·GaMe$_3$ (**3**) and SIPr·GaMe$_3$ (**4**). Selected bond lengths (Å) and angles (°) for **1**: Ga(1)−C(1) 2.111(2), C(1)−Ga(1)−C(2) 108.8(1), C(1)−Ga(1)−C(3) 105.8(1), C(2)−Ga(1)−C(3) 111.1(1), C(3)−Ga(1)−C(3A) 114.0(2). Selected bond lengths (Å) and angles (°) for **2**: Ga(1)−C(1) 2.124(5), C(1)−Ga(1)−C(2) 105.0(2), C(1)−Ga(1)−C(3) 110.8(2), C(1)−Ga(1)−C(4) 106.8(2), C(2)−Ga(1)−C(3) 112.5(2), C(2)−Ga(1)−C(4) 113.1(2), C(3)−Ga(1)−C(4) 108.5(3). Selected bond lengths (Å) and angles (°) for **3**: Ga(1)−C(1) 2.105(4), C(1)−Ga(1)−C(2) 101.3(1), C(1)−Ga(1)−C(3) 110.7(1), C(1)−Ga(1)−C(4) 108.4(2), C(2)−Ga(1)−C(3) 115.3(2), C(2)−Ga(1)−C(4) 112.4(2), C(3)−Ga(1)−C(4) 108.3(2). Selected bond lengths (Å) and angles (°) for **4**: Ga(1)−C(1) 2.137(2), C(1)−Ga(1)−C(2) 100.0(1), C(1)−Ga(1)−C(3) 111.2(1), C(1)−Ga(1)−C(4) 107.5(1), C(2)−Ga(1)−C(3) 110.4(1), C(2)−Ga(1)−C(4) 115.1(1), C(3)−Ga(1)−C(4) 112.1(1). Thermal ellipsoids are drawn at the 50% probability level. Hydrogen atoms have been omitted for clarity.

Fig. 5 Molecular structures of IMes·InMe$_3$ (**5**), SIMes·InMe$_3$ (**6**), IPr·InMe$_3$ (**3**) and SIPr·InMe$_3$ (**8**). Selected bond lengths (Å) and angles (°) for **5**: In(1)−C(1) 2.304(8), C(1)−In(1)−C(2) 105.5(3), C(1)−In(1)−C(3) 105.2(3), C(1)−In(1)−C(4) 104.3(3), C(2)−In(1)−C(3) 114.7(3), C(2)−In(1)−C(4) 111.0(4), C(3)−In(1)−C(4) 114.9(4). Selected bond lengths (Å) and angles (°) **6**: In(1)−C(1) 2.316(8), C(1)−In(1)−C(2) 105.9(3), C(1)−In(1)−C(3) 109.2(3), C(1)−In(1)−C(4) 101.8(3), C(2)−In(1)−C(3) 109.7(4), C(2)−In(1)−C(4) 114.1(3), C(3)−In(1)−C(4) 115.3(3). Selected bond lengths (Å) and angles (°) for **7**: In(1)−C(1) 2.309(2), C(1)−In(1)−C(2) 106.8(1), C(1)−In(1)−C(3) 108.6(1), C(1)−In(1)−C(4) 101.3(1), C(2)−In(1)−C(3) 111.4(1), C(2)−In(1)−C(4) 114.5(1), C(3)−In(1)−C(4) 113.3(1). Selected bond lengths (Å) and angles (°) for **8**: In(1)−C(1) 2.342(2), C(1)−In(1)−C(2) 99.6(1), C(1)−In(1)−C(3) 104.8(1), C(1)−In(1)−C(4) 108.5(1), C(2)−In(1)−C(3) 119.1(1), C(2)−In(1)−C(4) 109.8(1), C(3)−In(1)−C(4) 113.5(1). Thermal ellipsoids are drawn at the 50% probability level. Hydrogen atoms have been omitted for clarity.

Table 1 Selected M–$C_{carbene}$ bond lengths for selected NHC group 13 alkyl complexes. For depicted structures see Fig. 2 and 3

	Formulae	Complex	M–$C_{carbene}$ [Å]
1	IMes·GaMe$_3$	**1**	2.111(2)
2	SIMes·GaMe$_3$	**2**	2.124(5)
3	IPr·GaMe$_3$	**3**	2.105(4)
4	SIPr·GaMe$_3$	**4**	2.137(2)
5	IMes·InMe$_3$	**5**	2.304(7)
6	SIMes·InMe$_3$	**6**	2.316(8)
7	IPr·InMe$_3$	**7**	2.309(2)
8	SIPr·InMe$_3$	**8**	2.342(2)
9	IMes·AlMe$_3$	**A**[6b]	2.098(2)
10	SIMes·AlMe$_3$	**B**[6b]	2.112(6)
11	IPr·AlMe$_3$	**C**[6b]	2.103(3)
12	SIPr·AlMe$_3$	**D**[6b]	2.127(2)
13	IiPrMe·GaMe$_3$ [a]	**E**[4f]	2.130(2)
14	IMes·GaMe$_2$OMe	**H**[4a]	2.089(2)
15	SIPr·GaMe$_3$	**I**[4a]	2.132(3)
16	SIMes[(CH$_2$)$_2$]^L·GaMe$_2$	**L**[4b]	2.079(1)
17	SIMes[(CH$_2$)$_3$]^L·GaMe$_2$·GaMe$_3$	**M**[4b]	2.087(1)
18	SIMes[Ar']^L·GaMe$_2$	**N**[4b]	2.080(1)
19	SIMes[Ar']^L·GaMe$_2$·GaMe$_3$	**N'**[4b]	2.070(1)
20	SIPr[Ar']^L·GaMe$_2$	**O**[4b]	2.066(1)
21	SIPr[Ar'']^L·GaMe$_2$	**P**[4b]	2.056(1)
22	IMes·InMe$_2$Cl	**R**[4d]	2.267(2)
23	IMes·InMe$_2$OTf	**S**[4d]	2.264(2)
24	IMes·InMe(OTf)$_2$	**T**[4d]	2.183(2)

[a] See abbreviations.

Table 2 Selected ^{1}H and ^{13}C NMR chemical shifts for complexes **1–8**

Complexes	^{1}H [InCH$_3$] (ppm)	^{13}C [MC$_{carbene}$] (ppm)	^{13}C [C$_{carbene}$][a] (ppm)
1	−0.56	181.7	219.4
2	−0.60	206.1	243.8
3	−0.59	184.5	220.4
4	−0.58	209.0	244.0
5	−0.52	—	219.4
6	−0.58	209.3	243.8
7	−0.60	186.8	220.4
8	−0.62	211.7	244.0
E[4f]	−0.10	176.8	207.5
F[5b]	0.27	183.7	212.9
Q[5b]	0.21	183.4	212.9

[a] ^{13}C NMR chemical shifts were obtained from ref. 15.

Spectroscopic studies of complexes 1–8

The ^{1}H and ^{13}C{^{1}H} NMR spectra obtained for complexes **1–8** are consistent with the low-temperature X-ray crystallographic analyses. The ^{1}H NMR spectra for the gallium and indium complexes display singlets ranging from δ_H −0.56 to −0.60, and δ_H −0.52 to −0.62 ppm, respectively, which is indicative of the presence of the methyl substituents on the metal centre. This is further corroborated by ^{13}C{^{1}H} NMR spectra which display singlets at δ_C −5.2 to −6.1 and δ_C −9.6 to −11 ppm for gallium and indium complexes, respectively. Furthermore, the IR spectra of **1–4** show a relatively strong stretching signal at around 524 cm^{-1}, consistent with the presence of the methyl groups on the metal centre.[14] Unfortunately, in the case of indium analogues, no suitable IR stretching signals were clearly observed, since the In–Me range falls within a high noise background region (i.e., ~400 cm^{-1}).[14] An upfield shift of the $C_{carbene}$ signals provides further confirmation of the complexes, as observed with other reported trimethylgallium and indium complexes (Table 2).[6b,15] Despite several attempts, no $C_{carbene}$ signal was obtained for complex **5**, presumably due to the large quadrupole moment of the indium centre.[4,7]

Lewis acid–Lewis base properties

The majority of previously reported NHC–gallium and –indium complexes comprise halide and hydride derivatives (NHC·MH$_{3-n}$Cl$_n$; M = Ga and In; n = 1, 2).[7] For example, the chlorogallane complexes IMes·GaH$_2$Cl and IMes·GaHCl$_2$ displayed increased Lewis acidity of the metal centre in the presence of increasing electron withdrawing groups (i.e., chloride atoms), consequently shortening the Ga–$C_{carbene}$ bond length,

and strengthening the gallium hydride bond (Table S3,† entries 10 and 11).[7i] The same effect has also been observed for the lighter counterparts IMes·AlH$_2$Cl and IMes·AlHCl$_2$, which result in significantly different catalytic activities in hydroalumination reactions (vide supra).[7g] With the inclusion of the herein reported trimethylgallium and indium complexes, a more complete perspective can be gained regarding substituent effects on the structural properties of group 13 NHC complexes by comparison with previously reported halide and hydride counterparts. As expected, in complexes **1** to **4**, the trimethylgallium moiety proves to be a poorer Lewis acid compared to its hydride and halide analogues. This is evident from the Ga–$C_{carbene}$ bond distances reported for the IMes, SIMes and IPr compounds (see the ESI,† entries 1–3 and 9–14). A similar trend can be established in the case of indium complexes – Lewis acid strength in the increasing order: MMe$_3$ < MH$_3$ < MX$_3$. The reported In–$C_{carbene}$ bond distances are shown in Table S3† (entries 5, 7 and 15–19).[7]

The $C_{carbene}$ ^{13}C NMR chemical shift is sensitive to the extent of the metal centre Lewis acidity, which in turn is directed by the donor ability of the ligands surrounding the metal centre. The majority of previously reported NHC gallium and indium complexes failed to exhibit an M–$C_{carbene}$ signal in their ^{13}C{^{1}H} NMR spectra, due to the quadrupolar moment of the metal centre.[4,7] Indeed, $C_{carbene}$ signals of only one gallium and one indium NHC complex (IMes·GaClH$_2$ and IMes·InMe$_2$Cl) have been reported (δ_C 172.5 and 177.5 ppm, respectively).[4d,7i] The $C_{carbene}$ ^{13}C{^{1}H} NMR signal of the complexes **1–4** and **6–8** (see Table 2) are relatively downfield compared to the gallium and indium complexes IMes·GaClH$_2$ and IMes·InMe$_2$Cl. This is anticipated, given that the presence of the chlorido ligand(s) on the metal centre exerts a strong electron-withdrawing effect and further corroborates that the MMe$_3$ moiety (M = Ga and In) is a poorer electron acceptor compared to MH$_3$ and MX$_3$. Jones et al. showed that reactions of potentially chelating bidentate bis-NHC or monodentate NHC ligands in 1 : 1 and 1 : 2 ratios, respectively, with indium halides produce pentacoordinate trigonal bipyramidal chelate or 2 : 1 NHC adducts, whereas hydrides only form monomeric tetracoordinate tetrahedral compounds due to the higher

Lewis acidity of the former.[7o,t] Since trimethylindium derivatives are expected to be poorer Lewis acids than indium halides, only monomeric tetracoordinate tetrahedral species would be anticipated. Therefore, two equivalents of the IMes free carbene were reacted with trimethylindium under various experimental conditions; however, despite several attempts pentacoordinate trigonal bipyramidal adducts were unable to be isolated supporting our initial prediction.

Stability studies

We have reported that for the lighter trimethylaluminium compounds **A–D**, the NHC steric bulk plays a significant role in determining the resulting complex stability. Complexes containing less sterically hindered NHC moieties, *i.e.* **A** and **B** (IMes and SIMes, respectively), are relatively stable in their solid state and can be stored for prolonged periods under nitrogen without any signs of decomposition, whereas complexes containing bulkier NHC ligands, *i.e.* **C** and **D** (IPr and SIPr, respectively), slowly decompose to their respective imidazolylidene and imidazolinylidene over time.[6b] These stability differences were attributed to the larger percent buried volume ($\%V_{Bur}$) occupied by the NHC ligands of **C** and **D** (IPr and SIPr), compared to those of **A** and **B** (IMes and SIMes),[6b,16] indicating that subtle variations in the steric bulk of the NHC substituent ($\Delta\%V_{Bur}$ *ca.* 2–4%) profoundly impact the overall complex stability. Additional insights gleaned by Hevia *et al.*[5a] and Dagorne *et al.*[5b] showed that bulky *n*NHC group 13 complexes, such as IPrGa·(CH$_2$SiMe$_3$)$_3$, I*t*Bu·GaMe$_3$ (**F**) and I*t*Bu·InMe$_3$ (**Q**) all isomerize to their respective *a*NHC counterparts, with the latter two isomerizing too rapidly to allow characterization in their normal form. Theoretical DFT calculations performed for normal and abnormal model complexes of **F** and **Q** revealed that the latter are more stable with a Gibbs free energy of −24.6 kJ mol^{-1} and −5.8 kJ mol^{-1} for *n***F** *vs.* *a***F** and *n***Q** *vs.* *a***Q**, respectively.

The mechanism proposed for the model complex IPrGa·(CH$_2$SiMe$_3$)$_3$ involves an initial dissociation to generate the free carbene and subsequent formation of the abnormal carbene species. In the case of our complexes **C** and **D**, solid crystalline samples stored under nitrogen showed decomposition into the free carbene alongside other unidentifiable species in their NMR spectra.[6b] In the case of the heavier Ga and In counterparts, compounds **1–8** showed relatively greater stability compared to their lighter analogues, with signs of decomposition observed only in the case of compounds **4** and **8**. However, signals indicative of the formation of abnormal species for the reported metal complexes were not observed throughout our ^{1}H NMR studies.

In order to elucidate the stability trends within the triad, $\%V_{Bur}$ calculations were undertaken with the M–C$_{carbene}$ bond distance fixed as the value obtained from our X-ray studies, and the bond length set at 2.0 Å – to enable a comparison between the various NHC ligands unbiased by variable M–NHC bond distances (see Table 3).[16] In agreement with the calculated dissociation energies, the $\%V_{Bur}$ increases gradually from **1** to **4** and **5** to **8** for the gallium and indium complexes,

respectively. Consequently, the relatively low stability observed for **4** and **8** may be qualitatively rationalized by the larger volume occupied by isopropylphenyl groups compared to the mesityl groups present in the NHC moieties.[6b] In a quantitative comparison between stable and unstable complexes – *i.e.*, IPr *vs.* SIPr, **3** *vs.* **4** and **7** *vs.* **8** – *ca.* 8.5% and 10.6% $\Delta\%V_{Bur}$ variances are observed for Ga and In, respectively – slightly greater than those found for their lighter Al counterparts (*ca.* 4%).[6b]

To gain a more thorough insight into the NHC structure–stability relationships, we calculated the DFT optimized structures for complexes **1–8** and our previously reported complexes **A–D**. For completeness, we extended this study to include IPr·Ga(CH$_2$SiMe$_3$)$_3$ and the hypothetical I*t*Bu trimethylgallium and indium *n*NHC complexes (**F** and **Q**, respectively)[5b] (see Table 3). Theoretical parameters were consistent with the observed experimental trends, however, the calculated $\Delta\%V_{Bur}$ reduced to only *ca.* 3.7% and 3.1%, for gallium and indium, respectively.

Inclusion of the hypothetical complex *n***F** produced a $\Delta\%V_{Bur}$ of *ca.* 7% in comparison with the stable complex **3**. This relatively minor discrepancy in $\%V_{Bur}$ has a pronounced effect in terms of dissociation energy, which is less than half for **F** than **3** (*cf.* 65.2 kJ mol^{-1} and 34.2 kJ mol^{-1}, respectively). Furthermore, the unstable complex **4**, similar in steric bulk to **F** ($\%V_{Bur}$ of 35.6% and 36.7%, respectively) has a significantly lower dissociation energy compared to complex **4** (*cf.* 34.2 kJ mol^{-1} and 52.8 kJ mol^{-1} for **F** and **4**, respectively). These observations are in line with those we reported for Al complexes SIPr·AlMe$_3$ (**D**) and I*t*Bu·AlMe$_3$ (*cf.* $\%V_{Bur}$ and E_{diss} for complexes **D** and I*t*Bu·AlMe$_3$ are 35.5%, 77.8 kJ mol^{-1} and 36.9%, 46.2 kJ mol^{-1}, respectively) attributed to the varying electron donating properties of the SIPr and I*t*Bu NHC moieties to the metal centre.[6b]

The DFT calculated $\%V_{Bur}$ between complexes **4** and **8** and their I*t*Bu analogues *n***F** and *n***Q** showed comparable values (*cf.* 35.6%, 36.2%, 36.7% and 37.5% **4**, **8**, **F** and **Q** respectively). The slightly lower values observed for **4** and **8** are in accordance with their greater stability in the normal NHC form compared to *n***F** and *n***Q**, which readily isomerize to their abnormal form.[5b] Unfortunately, all attempts to isolate metal-containing species resulting from the structural decay of complexes **4** and **8** were unsuccessful.

Our calculations indicate that the facile isomerization of the previously reported IPr·Ga(CH$_2$SiMe$_3$)$_3$ [5a] to its abnormal isomeric form can be attributed to the higher steric congestion imposed by the CH$_2$SiMe$_3$ group when compared to Me groups ($\%V_{Bur}$ 64.5% and 48.7% for CH$_2$SiMe$_3$ and Me groups). This is further illustrated by the longer Ga–C$_{carbene}$ bond distance and lower dissociation energies calculated for IPr·Ga(CH$_2$SiMe$_3$)$_3$ and IPr·GaMe$_3$ (**3**) (*cf.*, 2.196(2) Å *vs.* 2.105(4) Å and 65.2 kJ mol^{-1} *vs.* 23.3 kJ mol^{-1}, respectively).

Comparative analysis of a stable *vs.* an unstable system using topographic steric maps of saturated complexes **2** *vs.* **4** and **6** *vs.* **8** showed that the distribution of steric bulk of the SIMes ligand in **2** and **6** is symmetrical around the metal,

Table 3 M–C$_{(carbene)}$ bond lengths, %V_{Bur} (X-ray and DFT) and dissociation energies for selected complexes

Entries	Complexes	M–C$_{carbene}$ [Å] X-Ray	M–C$_{carbene}$ [Å] DFT	%V_{Bur} R = X-ray	%V_{Bur} R = 2.0 Å (X-ray)	%V_{Bur} R = DFT	%V_{Bur} R = 2.0 Å (DFT)	E_{diss} (kJ mol^{-1})
1	**1**	2.111(2)	2.201	27.9	29.6	29.5	32.7	76.7
2	**2**	2.125(5)	2.231	31.8	34.1	30.2	33.9	69.0
3	**3**	2.105(4)	2.213	34.0	36.2	30.9	34.3	65.2
4	**4**	2.137(2)	2.233	35.1	39.3	31.9	35.6	52.8
5	**5**	2.301(8)	2.428	28.5	34.0	25.7	33.3	73.9
6	**6**	2.316(8)	2.453	29.2	34.9	26.3	34.4	66.8
7	**7**	2.309(2)	2.446	30.2	35.7	27.1	35.1	61.5
8	**8**	2.342(2)	2.478	31.4	39.5	27.7	36.2	51.3
9	**A** [6b]	2.098(2)	2.162	31.7	33.7	28.9	32.8	105.2
10	**B** [6b]	2.112(6)	2.188	32.0	34.1	30.4	33.8	95.6
11	**C** [6b]	2.103(3)	2.164	33.1	35.0	31.2	34.3	93.5
12	**D** [6b]	2.127(2)	2.190	36.1	38.5	32.0	35.5	77.8
13	**E** [4f]	2.130(2)	2.165	—	—	25.5	27.8	90.3
14[a]	**F** [5b]	—	2.316	—	—	31.6	36.7	34.2
15[a]	**Q** [5b]	—	2.558	—	—	28.4	37.5	20.5
16	IPr·Ga(CH$_2$SiMe$_3$)$_3$ [5a]	2.196(2)	2.301	31.9	36.1	26.2	31.6	23.3

%V_{Bur} Me groups on IPr–GaR$_3$ = 48.7. %V_{Bur} CH$_2$SiMe$_3$ groups on IPr–GaR$_3$ = 64.5. [a] %V_{Bur} was performed on DFT optimized structure (No single crystal X-ray structures were obtained).

whereas for **4** and **8**, localization of steric hindrance around the bulkier *ortho* isopropyl group was clearly observed on the steric contour map (see Fig. 6 and the ESI†). This asymmetric spatial distribution of the NHC ligand around the metal centres in **4** and **8** correlates with their reduced stability compared to **2** and **6** respectively (see the ESI†).

Bonding studies

To gain a better understanding of the nature of M–NHC bonds with M = Al, Ga and In, bond snapping energy (BSE) analysis was performed.[16] The BSE is the energy required for the dissociation of the M–L bond, analysed based on the interaction between fragments possessing both the local equilibrium geometry of the final molecule and an electronic structure suitable for bond formation. To calculate the heterolytic BSE for **1–8**, the geometry of the metal fragment [M] – in this case MMe$_3$ – was fixed, and the complex fragmented into its corresponding neutral [M] and NHC components.

Although BSE does not correlate in all instances with bond dissociation enthalpies (since reorganization and relaxation of the fragments are not considered), it closely relates to bond

enthalpy terms, providing a good approximation to bond strength values.

The BSE can be decomposed into two main terms, namely steric interaction (ΔE_0) and orbital interaction (ΔE_{int}) (eqn (1)):[17]

$$BSE = -[\Delta E_0 + \Delta E_{int}] \tag{1}$$

The steric interaction term ΔE_0 can be further split into an electrostatic interaction term ΔE_{elstat} and a Pauli repulsion term ΔE_{Pauli} (eqn (2)):[17]

$$\Delta E_0 = \Delta E_{elstat} + \Delta E_{Pauli} \tag{2}$$

The ΔE_{Pauli} repulsion term describes the two-orbital electron interactions between the occupied orbitals of both fragments. The ΔE_{elstat} and ΔE_{Pauli} terms constitute stabilizing and destabilizing contributions to BSE, respectively, with their relative contributions determining the overall character of ΔE_0.

The ΔE_{int} term may also be further broken down into contributions from the respective orbital interactions within the various irreducible representations τ of the overall symmetry group of the system (eqn (3)):[17]

$$\Delta E_{int} = \Sigma_\tau \Delta E_{int}^\tau \tag{3}$$

Each complex studied in the present work, **1–8**, has been optimized with a C_s imposed symmetry, where the NHC ligands are positioned in the σ_{xy} mirror plane of the molecule. Therefore, the A′ contributions to the orbital interaction energy are associated with σ-bonding, whereas the A″ contributions represent π-interactions. The A″ contribution of the orbital interaction energy may be further divided into NHC → M π–donation, $\Delta E_{int}^\pi {}_{C \to M}$, and M → NHC π-backdonation, $\Delta E_{int}^\pi {}_{M \to C}$. To estimate these two interactions, additional constrained space orbital variation (CSOV) calculations were performed.[17] In particular, to assess the contribution of π-donation, bond decomposition analysis was performed by considering the interaction of a [M] fragment and an NHC
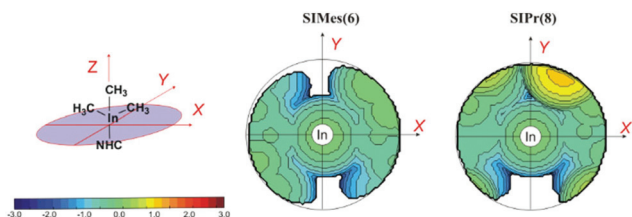
Fig. 6 Topographic steric maps of the SIMes and SIPr ligands in **6** and **8**. The iso-contour curves of the steric maps are in Å. The maps have been obtained starting from the crystallographic data of the Al–NHC complexes (CIF), with the Al–C$_{carbene}$ distance fixed at 2.0 Å. The *xz* plane is the mean plane of the NHC ring, whereas the *yz* plane is the plane orthogonal to the mean plane of the NHC ring, and passing through the C$_{carbene}$ atom of the NHC ring.

ligand, excluding the set of virtual A″ orbitals of the NHC fragment from the variational space. In this way, the A″ contribution of the orbital interaction energy is associated only with the NHC → [M] A″ donation, or π-donation. Similarly, the level of π back-donation was determined by explicitly excluding all virtual A″ orbitals on the [TM] fragment.

The energy decomposition analysis (EDA) is performed in the gas phase since it refers to the intrinsic strength of the M–NHC bond, which is independent of the environment that may stabilize the two fragments. We selected one NHC ligand, namely IMes, as a case study for comparison between three metals (see Table 4). The data reported in Table 4 suggest that the greater strength of the Al–IMes bond with respect to that of the Ga–IMes bond is mainly attributable to the steric term (ΔE_0). In fact, the Pauli contribution of the steric term, ΔE_{Pauli}, destabilizes the Ga system more than the electrostatic term does, with $\Delta(\Delta E_{\text{Pauli}}(\text{Ga}) - \Delta E_{\text{Pauli}}(\text{Al}))$ being almost 3.5 times larger with respect to $\Delta(\Delta E_{\text{elstat}}(\text{Ga}) - \Delta E_{\text{elstat}}(\text{Al}))$. As a result, the steric term disfavours the Ga–IMes bond by 45.7 kJ mol^{-1}. This is in agreement with theoretical studies by Frenking *et al.* on a series of IMe NHC group 13 metal hydride complexes.[18] Our detailed orbital analysis shows that the greater ΔE_{Pauli} term for the Ga–IMes system is related to the interactions between the occupied orbitals on the NHC and the occupied 3d orbitals on the Ga atom whereby the smaller ΔE_{Pauli} for Al is due to the lack of available d-electrons. Intuitively, the orbital interaction is primarily constituted by the σ term, which is larger in magnitude for the Ga–IMes system, as also seen for IMe·GaH$_3$[18] compared to its Al counterpart (see Table 4). For the π term, the main difference is in the M → C interaction, *i.e.* almost 4 kJ mol^{-1} stronger for Al.

In a comparison of Ga *vs.* In, the steric term (ΔE_0) once again disfavors the Ga system. In this case, the ΔE_{Pauli} term has the greatest contribution, with $\Delta(\Delta E_{\text{Pauli}}(\text{Ga}) - \Delta E_{\text{Pauli}}(\text{In}))$ being 1.5 times greater with respect to the electrostatic $\Delta(\Delta E_{\text{elstat}}(\text{Ga}) - \Delta E_{\text{elstat}}(\text{In}))$. The orbital interaction is much greater for the Ga–IMes bond, both at the σ and π levels, compensating for the unfavored steric term. Similarly, this was reported for the computed IMe·GaH$_3$ complex and its In analogue.[18] For completeness, it is worth noting that the greater BSE observed for the Al–NHC bond, with respect to that of Ga–NHC, reflects the larger E_{diss} associated with Al compounds compared to Ga (see the last column in Table 3). With

regard to the Ga/In trend, the dissociation energies are almost identical (varying less than 4.0 kJ mol^{-1}), in agreement with the smaller discrepancy between the BSE for the Ga/In–NHC bonds with respect to the Al/Ga–NHC bonds (*i.e.* 20 kJ mol^{-1} and 30 kJ mol^{-1} for Al and Ga, respectively).

Further group 13 bonding insights can be gained from the ^{1}H and ^{13}C NMR spectra. Hence, DFT-NMR analyses were performed for the C$_{\text{carbene}}$ and Me group hydrogen atoms in the complexes IMes·AlMe$_3$ (**A**) and SIMes·AlMe$_3$ (**B**) to predict their ^{13}C and ^{1}H NMR spectra. The calculated chemical shielding (σ_C) is −3.9 and −24.3 ppm for the C$_{\text{carbene}}$ atom of the IMes and SIMes system, respectively. Decomposition of the isotropic σ_C into dia- and paramagnetic terms, $\sigma_C = \sigma_d + \sigma_p$, indicates that the change in σ_C is mainly due to the paramagnetic term σ_p, that varies by almost 21 ppm downfield from IMes to SIMes. Previous literature[19] has indicated that the carbene chemical shift in NHC ligands is related to transitions between the filled σ orbitals of the M–NHC bond (HOMO) and the empty π orbital of the carbene (LUMO). Hence, we undertook analyses on the HOMO–LUMO energies of the NHC ligand showing that the energy gap decreases by almost 0.2 eV from IMes to SIMes. This can be attributed to a decreased stability of the SIMes NHC molecule HOMO, which results in a stronger magnetic coupling, and additionally accounts for the higher paramagnetic shielding (corresponding downfield shift) in Al–SIMes with respect to Al–IMes. The DFT ^{1}H NMR analysis revealed that the upfield shift of the SIMes·AlMe$_3$ methyl hydrogens corresponds to a reduced π back-donation [Al] → NHC (π*) that results from a smaller π orbital overlap, probably as a consequence of the slightly elongated Al–SIMes bond distance. As a result of this decreased [Al] → NHC back-donation, electron density is pushed towards neighbouring ligands on the Al centre, *i.e.* the methyl groups, thus leading to an upfield shift of the H atoms.

Our EDA results highlight that the interactions between the occupied orbitals on the NHC and the occupied Ga 3d orbitals destabilize this system with respect to the Al and In counterparts. However, a stronger orbital interaction for Ga compared to In sets the trend of the total M–NHC bond strength as Al > Ga > In. The overall orbital interaction is primarily constituted by the σ term, with a relatively small π term that consists mostly of a back-donation from the metal fragment to the NHC. To further extend our comparison and quantify the existing bonding discrepancies between our main group NHC complexes and well-established transition metal (TM)–NHC and –PHC systems, BSE decomposition analyses were performed, implementing IMes–Pd–IMes and IMes(P)–Pd–(P)IMes as case studies (see Table 5).

The increased strength of the Pd–NHC bond (almost 30.0 kJ mol^{-1}) with respect to that of Al–NHC is largely attributed to the steric term (20.0 kJ mol^{-1}) rather than to the orbital interaction (10 kJ mol^{-1}). For the latter contribution, despite a smaller σ term in the Pd–NHC bond, a two-fold greater π term is found due to π back-donation. In the case of the Pd–PHC system, the considered bond bears a greater resemblance to that of Al–NHC for the steric and σ terms, and as expected, a

Table 4 EDA results (in kJ·mol^{-1}) of M–IMes bond (M = Al, Ga and In) complexes

	A (Al)	**1** (Ga)	**5** (In)
ΔE_0	10.0	45.7	20.3
ΔE_{elstat}	−321.4	−334.7	−287.6
ΔE_{Pauli}	331.4	380.4	308.0
ΔE_{int}	−175.4	−180.8	−135.5
$\sigma - \Delta E_{\text{int}}$	−151.3 (86.3%)	−161.4 (89.3%)	−119.8 (88.5%)
$\pi - \Delta E_{\text{int}}$	−24.1 (13.7%)	−19.4 (10.7%)	−15.6 (11.5%)
$\Delta E^{\pi}_{\text{int C}\rightarrow\text{M}}$	−8.5	−7.3	−5.5
$\Delta E^{\pi}_{\text{int M}\rightarrow\text{C}}$	−18.1	−14.3	−11.4
BSE	165.3	135.1	115.2

Table 5 BSE-decomposition (in kJ mol^{-1}) of Al–IMes, Pd–IMes and Pd–(P)IMes bonds

	Al–IMes	Pd–IMes	Pd–(P)IMes
ΔE_{elstat}	−321.4	−589.4	−537.3
ΔE_{Pauli}	331.4	578.3	550.6
ΔE_0	10.0	−11.1	13.3
ΔE_{int}	−175.4	−182.7	−196.7
$\sigma - \Delta E_{int}$	−151.3 (86.3%)	−129.0 (70.6%)	−143.2 (72.8%)
$\pi - \Delta E_{int}$	−24.1 (13.7%)	−53.8 (29.4%)	−53.5 (27.2%)
$\Delta E^{\pi}_{int\ C \rightarrow M}$	−8.5	−5.8	−5.6
$\Delta E^{\pi}_{int\ M \rightarrow C}$	−18.1	−50.6	−49.6
BSE	165.3	193.8	183.4

significant π back-donation term, similar to the case of Pd–NHC is found. Substitution of N with P atoms results in both strengthening of the orbital contribution (σ term) and disfavouring of the steric term (mainly Pauli term) to the M–NHC bond.

Conclusions

The present work describes the synthesis and characterization of a series of new aromatic *N*-substituted NHC trimethylgallium and indium species. Similarly to their aluminium counterparts, these complexes exhibit varying stabilities, which are attributed to small differences in the steric bulk of the chosen NHC. Our computational study has allowed quantification and rationalisation of discrepancies between M–NHC bond strengths for the Al, Ga, and In triad. Moreover, a quantitative comparison with well-established transition metal systems (Pd–NHC and –PHC) determines that an increase in both the electrostatic interaction and [M] → NHC π back-bonding is largely responsible for the existing differences between group 13 and transition metal NHC complexes.

Experimental section

General procedures

All manipulations were carried out using standard Schlenk and glove-box techniques under a dried-argon atmosphere and using oven-dried glassware. Ether and toluene were distilled over Na/benzophenone, degassed and purged with dry argon prior to use, and stored under 4 Å molecular sieves. Deuterated benzene, C$_6$D$_6$, was distilled over Na and stored under a potassium mirror. Acetonitrile, for high-resolution mass spectrometry, was stirred over 4 Å molecular sieves, subsequently distilled over CaH$_2$ prior to use, and stored under 4 Å molecular sieves. Starting materials, IMes, SIMes, IPr, and SIPr were prepared as previously described.[13,22] Trimethylgallium was synthesized by first dissolving gallium trichloride (5.00 g, 28.40 mmol) in 5 mL of degassed toluene followed by dropwise addition of the mixture degassed triethylamine (4.44 g, 43.89 mmol) and trimethylaluminium (3.16 g, 43.89 mmol). Following the addition, the reaction was stirred

overnight and distilled at atmospheric pressure to obtain the neat trimethylgallium.[7] A solution of trimethylgallium (0.702 M) in toluene was then prepared from the distilled trimethylgallium. Trimethylindium was generated *in situ* by reacting MeLi (3 M in DME) with InCl$_3$ (0.221 g, 1 mmol) dissolved in ether at −78 °C and filtered through Celite before addition to the carbene.[8]

Instrumentation

^{1}H (400 MHz), ^{13}C NMR (100/125 MHz) spectra were recorded using Bruker Avance DPX400 and 500 spectrometers with the ^{1}H, ^{13}C NMR chemical shifts internally referenced to the residual solvent used. All NMR spectroscopic analyses were performed at room temperature (300 K). High-resolution mass spectra were obtained by using a Water Q-Tof Premier, with ESI mode. Melting points were determined on a SRS-Optimelt MPA-100 apparatus using sealed glass capillaries under argon and were uncorrected. Infrared spectra were recorded as Nujol mulls by using NaCl plates on a Shimadzu IR Prestige-21 FTIR spectrometer.

Procedure for the synthesis of complexes 1–8

IMes·GaMe$_3$ (1). IMes (0.304 g, 1 mmol) was dissolved in toluene followed by the addition of trimethylgallium (GaMe$_3$), (1.45 mL, 1 mmol, 0.702 M in toluene) at room temperature. The resulting solution was stirred overnight at room temperature and later filtered through Celite to give a clear solution. The solvent was then evaporated to dryness, followed by the addition of ether to yield a saturated solution. Colourless crystals were grown at room temperature. Yield: 37%. Mp: 196–199 °C. ^{1}H NMR (400 MHz, C$_6$D$_6$): δ = −0.56 (s, 9H, GaMe$_3$), 2.01 (s, 12H, *o*-Ph(CH$_3$)), 2.09 (s, 6H, *p*-Ph(CH$_3$)), 6.02 (s, 2H, NCH), 6.76 (s, 4H, C$_6$H$_2$). ^{13}C{^{1}H} NMR (100 MHz, C$_6$D$_6$): δ = −6.1 (GaMe$_3$), 17.6 (ArMe), 21.0 (ArMe), 122.5 (NCH), 129.3 (*Ar*), 135.4 (*Ar*), 135.6 (*Ar*), 139.3 (*Ar*), 181.7 (C$_{carbene}$, weak). IR (Nujol, cm^{-1}): ṽ = 525 (ν Ga–C stretch; m). HRMS: calcd for C$_{24}$H$_{33}$GaN$_2$ [M + H]$^+$: 419.1978; found 419.1992.

SIMes·GaMe$_3$ (2). The same procedure was adopted as that for **1** except that colourless crystals were obtained in saturated toluene solution. Yield: 53%. Mp: 201–205 °C. ^{1}H NMR (400 MHz, C$_6$D$_6$): δ = −0.60 (s, 9H, GaMe$_3$), 2.08 (s, 6H, *p*-Ph(CH$_3$)), 2.21 (s, 12H, *o*-Ph(CH$_3$)), 3.02 (s, 4H, NCH$_2$), 6.77 (s, 4H, C$_6$H$_2$). ^{13}C{^{1}H} NMR (100 MHz, C$_6$D$_6$): δ = −5.9 (GaMe$_3$), 17.9 (ArMe), 21.0 (ArMe), 50.9 (NCH), 129.7 (*Ar*), 135.6 (*Ar*), 136.1 (*Ar*), 138.4 (*Ar*), 206.1 (C$_{carbene}$, weak). IR (Nujol, cm^{-1}): ṽ = 525 (ν Ga–C stretch; s). HRMS: calcd for C$_{24}$H$_{35}$GaN$_2$ [M + H]$^+$: 421.2134; found 421.2140.

IPr·GaMe$_3$ (3). The same procedure was adopted as that for **1** except that colourless crystals were obtained in saturated toluene solution. Yield: 35%. Mp: 167–172 °C. ^{1}H NMR (400 MHz, C$_6$D$_6$): δ = −0.59 (s, 9H, GaMe$_3$), 0.99–1.00 (d, 12H, J_{H-H} = 6.8 Hz, CH(CH$_3$)$_2$), 1.38–1.40 (d, 12H, J_{H-H} = 6.8 Hz, CH(CH$_3$)$_2$), 2.75–2.82 (p, 4H, J_{H-H} = 6.8 Hz, CH(CH$_3$)$_2$), 6.46 (s, 2H, NCH$_2$), 7.11–7.13 (m, 4H, *m*-C$_6$H$_3$), 7.22–7.26 (m, 2H, *p*-C$_6$H$_3$). ^{13}C{^{1}H} NMR (100 MHz, C$_6$D$_6$): δ = −5.6 (GaMe$_3$), 22.8 (CH(CH$_3$)$_2$), 25.8 (CH(CH$_3$)$_2$), 28.8 (CH(CH$_3$)$_2$), 124.1 (*Ar*), 124.2

(Ar), 130.6 (NCH), 135.6 (Ar), 145.8 (Ar), 184.3 (C$_{carbene}$, weak). IR (Nujol, cm^{-1}): $\tilde{\nu}$ = 525 (ν Ga–C stretch; m). HRMS: calcd for C$_{30}$H$_{45}$GaN$_2$ [M + H]$^+$: 503.2917; found 503.2930.

SIPr·GaMe$_3$ (4). The same procedure was adopted as that for **1** except that colourless crystals were obtained in saturated toluene solution. Yield: 39%. Mp: 207–210 °C. ^{1}H NMR (400 MHz, C$_6$D$_6$): δ = −0.58 (s, 9H, GaMe_3), 1.15–1.17 (d, 12H, $J_{H–H}$ = 6.8 Hz, CH(CH_3)$_2$), 1.50–1.51 (d, 12H, $J_{H–H}$ = 6.8 Hz, CH (CH_3)$_2$), 3.28–3.35 (p, 4H, $J_{H–H}$ = 6.7 Hz, CH(CH$_3$)$_2$), 3.50 (s, 4H, NCH_2), 7.14–7.16 (m, 2H, p-C$_6$H$_3$), 7.21–7.27 (m, 4H, m-C$_6$H$_3$). ^{13}C{^{1}H} NMR (100 MHz, C$_6$D$_6$): δ = −5.2 (GaMe_3, broad), 23.7 (CH(CH$_3$)$_2$), 26.1 (CH(CH$_3$)$_2$), 28.8 (CH(CH$_3$)$_2$), 54.0 (NCH), 124.6 (Ar), 129.8 (Ar), 135.8 (Ar), 146.8 (Ar), 209.0 (C$_{carbene}$, weak). IR (Nujol, cm^{-1}): $\tilde{\nu}$ = 521 (ν Ga–C stretch; m). HRMS: calcd for C$_{30}$H$_{47}$GaN$_2$ [M + H]$^+$: 505.3073; found 505.3090.

IMes·InMe$_3$ (5). The compound IMes (0.304 g, 1 mmol) was dissolved in ether followed by the addition of *in situ* generated trimethylindium (InMe$_3$, 1 mmol) to the reaction mixture at 0 °C. The resulting solution was stirred overnight at 0 °C and later filtered through Celite to give a clear solution. The solution was concentrated and colourless crystals were grown at 0 °C. Yield: 34%. Mp: 172–179 °C. ^{1}H NMR (400 MHz, C$_6$D$_6$): δ = −0.52 (s, 9H, InMe_3), 1.99 (s, 12H, o-Ph(CH_3)), 2.09 (s, 6H, p-Ph(CH_3)), 6.03 (s, 2H, NCH), 6.77 (s, 4H, C$_6$H$_2$). ^{13}C{^{1}H} NMR (100 MHz, C$_6$D$_6$): δ = −11.0 (InMe_3), 17.6 (ArMe), 21.0 (ArMe), 122.5 (NCH), 129.4 (Ar), 135.3 (Ar), 135.6 (Ar), 139.4 (Ar). HRMS: calcd for C$_{24}$H$_{33}$InN$_2$ [M + H]$^+$: 465.1761; found 465.1757.

SIMes·InMe$_3$ (6). The same procedure was adopted as that for **5** but the reaction was conducted at room temperature. Colourless crystals were grown at room temperature (25 °C). Yield: 60%. Mp: 213–216 °C. ^{1}H NMR (400 MHz, C$_6$D$_6$): δ = −0.58 (s, 9H, InMe_3), 2.09 (s, 6H, p-Ph(CH_3)), 2.19 (s, 12H, o-Ph (CH_3)), 3.01 (s, 4H, NCH_2), 6.78 (s, 4H, C$_6$H$_2$). ^{13}C{^{1}H} NMR (100 MHz, C$_6$D$_6$): δ = −10.7 (InMe_3, broad), 17.9 (ArMe), 21.0 (ArMe), 50.9 (NCH), 129.9 (Ar), 135.5 (Ar), 136.1 (Ar), 138.5 (Ar), 209.3 (C$_{carbene}$, weak). HRMS: calcd for C$_{24}$H$_{35}$InN$_2$ [M + H]$^+$: 467.1917; found 467.1923.

IPr·InMe$_3$ (7). The same procedure was adopted as that for **5** but the reaction was conducted at room temperature. Colourless crystals were grown at 0 °C. Yield: 63%. Mp: 148–153 °C. ^{1}H NMR (400 MHz, C$_6$D$_6$): δ = −0.60 (s, 9H, InMe_3), 0.99–1.01 (d, 12H, $J_{H–H}$ = 6.8 Hz, CH(CH_3)$_2$), 1.36–1.38 (d, 12H, $J_{H–H}$ = 6.8 Hz, CH(CH_3)$_2$), 2.72–2.79 (p, 4H, $J_{H–H}$ = 6.9 Hz, CH(CH$_3$)$_2$), 6.48 (s, 2H, NCH_2), 7.11–7.13 (m, 4H, m-C$_6$H$_3$), 7.23–7.26 (m, 2H, p-C$_6$H$_3$). ^{13}C{^{1}H} NMR (100 MHz, C$_6$D$_6$): δ = −10.3 (InMe_3, broad), 23.1 (CH(CH$_3$)$_2$), 25.6 (CH (CH$_3$)$_2$), 28.8 (CH(CH$_3$)$_2$), 124.2 (Ar), 130.6 (NCH), 135.6 (Ar), 145.8 (Ar), 186.8 (C$_{carbene}$, weak). HRMS: calcd for C$_{30}$H$_{45}$InN$_2$ [M + H]$^+$: 549.2700; found 549.2704.

SIPr·InMe$_3$ (8). The compound SIPr (0.390 g, 1 mmol) was dissolved in ether followed by the addition of *in situ* generated trimethylindium (InMe$_3$, 1 mmol) to the reaction mixture at 0 °C. The resulting solution was stirred for 30 min at 0 °C, subsequently colourless crystals were formed. The solution was removed to isolate the crystals and later concentrated to yield

more compounds. Colourless crystals were grown at 0 °C. Yield: 36%. Mp: 194–200 °C. ^{1}H NMR (400 MHz, C$_6$D$_6$): δ = −0.62 (s, 9H, InMe_3), 1.10–1.11 (d, 12H, $J_{H–H}$ = 6.8 Hz, CH (CH_3)$_2$), 1.43–1.45 (d, 12H, $J_{H–H}$ = 6.8 Hz, CH(CH_3)$_2$), 3.19–3.26 (p, 4H, $J_{H–H}$ = 6.8 Hz, CH(CH$_3$)$_2$), 3.42 (s, 4H, NCH_2), 7.10–7.12 (m, 4H, m-C$_6$H$_3$), 7.19–7.23 (m, 2H, p-C$_6$H$_3$). ^{13}C{^{1}H} NMR (125 MHz, C$_6$D$_6$): δ = −9.6 (InMe_3, broad), 23.9 (CH(CH$_3$)$_2$), 25.9 (CH(CH$_3$)$_2$), 28.8 (CH(CH$_3$)$_2$), 54.1 (NCH), 124.7 (Ar), 129.9 (Ar), 135.7 (Ar), 146.8 (Ar), 211.7 (C$_{carbene}$, weak). HRMS: calcd for C$_{30}$H$_{47}$InN$_2$ [M + H]$^+$: 551.2856; found 551.2878.

X-ray crystallographic studies

Diffraction-quality crystals **1–8** were obtained in toluene or ether solvent at room temperature or 0 °C. The crystals were mounted onto quartz fibres, and the X-ray diffraction intensity data were obtained at 103 K with a Bruker Kappa diffractometer equipped with a CCD detector, employing Mo Kα radiation (λ = 0.71073 Å), with the SMART suite of programs.[20] All data were processed and corrected for Lorentz and polarization effects with SAINT and for absorption effects with SADABS.[21] Structural solution and refinement were carried out with the SHELXTL suite of programs.[22] The structures were solved by direct methods or Patterson maps to locate the heavy atoms, followed by difference maps for the light, non-hydrogen atoms. All non-hydrogen atoms were refined with anisotropic thermal parameters. The crystals of **7** had one disordered isopropyl group modelled in two alternative sites (with ~0.5 occupancy) and refined with appropriate restraints.

Computational details

All calculations have been performed with the Amsterdam Density Functional suite of programs, ADF.[23–25] Gradient-corrected density-functional calculations were based on the local density approximation with Slater exchange[26] and VWN correlation.[27] Gradient corrections for exchange and correlation were those proposed by Becke[28] and Perdew,[29] respectively. Valence electrons were described with an STO basis of triple-ζ quality, augmented by one polarization function.[30] Electrons of the core shells (1s2s2p for Al, 1s2s2p3s3p for Ga, 1s2s2p3s3p3d4s4p for In, 1s2s2p for P, 1s2s2p for Si, 1s for C and N) have been treated within the frozen core approximation.[23] Relativistic effects have been incorporated based on the zero-order regular approximation.

%V_{Bur} calculation parameters. All calculations were performed on DFT optimized structures using the SambVca program.[16b] The C$_{carbene}$ centre is coordinated at the origin of the sphere with a distance equal to the fixed value of 2.0 Å. 3.50 Å was selected as the value for the sphere radius; mesh spacing for numerical integration was scaled to 0.05; hydrogen atoms were omitted for the calculations; and bond radii were scaled by 1.17.

Abbreviations

IiPrMe   1,3-Isopropyl-4,5-dimethylimidazol-2-ylide-ne
ItBu   1,3-Di-*tert*-butylimidazol-2-ylidene

IMes   1,3-Bis-(2,4,6-trimethylphenyl)imidazol-2-ylidene
SIMes   1,3-Bis-(2,4,6-trimethylphenyl)imidazolin-2-ylidene
IPr   1,3-Bis-(2,6-diisopropylphenyl)imidazol-2-ylidene
SIPr   1,3-Bis-(2,6-diisopropylphenyl)imidazolin-2-ylidene
PHC   P-Heterocyclic carbene

Acknowledgements

Notes and references

1 L. Cavallo and C. S. J. Cazin, in *N-heterocyclic Carbenes in Transition Metal Catalysis and Organocatalysis*, ed. C. S. J. Cazin, Springer, Netherlands, 2011, vol. 32, pp. 1–22.

2 (*a*) D. Zhang and G. Zi, *Chem. Soc. Rev.*, 2015, **44**, 1898–1921; (*b*) S. Bellemin-Laponnaz and S. Dagorne, *Chem. Rev.*, 2014, **114**, 8747–8774; (*c*) S. J. Hock, L.-A. Schaper, W. A. Herrmann and F. E. Kühn, *Chem. Soc. Rev.*, 2013, **42**, 5073–5090; (*d*) V. P. Boyarskiy, K. V. Luzyanin and V. Y. Kukushkin, *Coord. Chem. Rev.*, 2012, **256**, 2029–2056; (*e*) H. D. Velazquez and F. Verpoort, *Chem. Soc. Rev.*, 2012, **41**, 7032–7060.

3 (*a*) C. Bour and V. Gandon, *Synlett*, 2015, 1427–1436; (*b*) C. Fliedel, G. Schnee, T. Avilés and S. Dagorne, *Coord. Chem. Rev.*, 2014, **275**, 63–86; (*c*) C. Bour and V. Gandon, *Coord. Chem. Rev.*, 2014, **279**, 43–57; (*d*) Y. Wang and G. H. Robinson, *Inorg. Chem.*, 2014, **53**, 11815–11832; (*e*) S. Aldridge and A. J. Downs, in *The Group 13 Metals Aluminium, Gallium, Indium and Thallium: Chemical Patterns and Peculiarities*, ed. S. Aldridge and A. J. Downs, Wiley, UK, 2011, vol. 3.

4 (*a*) P. Horeglad, M. Cybularczyk, B. Trzaskowski, G. Z. Żukowska, M. Dranka and J. Zachara, *Organometallics*, 2015, **34**, 3480–3496; (*b*) P. Horeglad, O. Ablialimov, G. Szczepaniak, A. M. Dąbrowska, M. Dranka and J. Zachara, *Organometallics*, 2014, **33**, 100–111; (*c*) P. Horeglad, G. Szczepaniak, M. Dranka and J. Zachara, *Chem. Commun.*, 2012, **48**, 1171–1173; (*d*) J. H. Cotgreave, D. Colclough, G. Kociok-Köhn, G. Ruggiero, C. G. Frost and A. S. Weller, *Dalton Trans.*, 2004, **10**, 1519–1520; (*e*) J. D. Gorden, C. L. B. Macdonald and A. H. Cowley, *J. Organomet. Chem.*, 2002, **643–644**, 487–489; (*f*) X.-W. Li, J. Su and G. H. Robinson, *Chem. Commun.*, 1996, **23**, 2683–2684.

5 (*a*) M. Uzelac, A. Hernán-Gómez, D. R. Armstrong, A. R. Kennedy and E. Hevia, *Chem. Sci.*, 2015, **6**, 5719–5728; (*b*) G. Schnee, O. N. Faza, D. Specklin, B. Jacques, L. Karmazin, R. Welter, C. S. López and S. Dagorne, *Chem. – Eur. J.*, 2015, **21**, 17959–17972.

6 (*a*) G. Schnee, D. Specklin, J.-P. Djukic and S. Dagorne, *Organometallics*, 2016, **35**, 1726–1734; (*b*) M. M. Wu, A. M. Gill, Y. Lu, L. Falivene, Y. Li, R. Ganguly, L. Cavallo and F. García, *Dalton Trans.*, 2015, **44**, 15166–15174; (*c*) R. A. Musgrave, R. S. P. Turberville, M. Irwin and J. M. Goicoechea, *Angew. Chem., Int. Ed.*, 2012, **51**, 10832–10835; (*d*) Y. Zhang, G. M. Miyake and E. Y.-X. Chen, *Angew. Chem., Int. Ed.*, 2010, **49**, 10158–10162; (*e*) A. R. Kennedy, R. E. Mulvey and S. D. Robertson, *Dalton Trans.*, 2010, **39**, 9091–9099; (*f*) A.-L. Schmitt, G. Schnee, R. Welter and S. Dagorne, *Chem. Commun.*, 2010, **46**, 2480–2482; (*g*) W.-C. Shih, C.-H. Wang, Y.-T. Chang, G. P. A. Yap and T.-G. Ong, *Organometallics*, 2009, **28**, 1060–1067; (*h*) Y. Lee, B. Li and A. H. Hoveyda, *J. Am. Chem. Soc.*, 2009, **131**, 11625–11633; (*i*) M. Schiefer, N. D. Reddy, H.-J. Ahn, A. Stasch, H. W. Roesky, A. C. Schlicker, H.-G. Schmidt, M. Noltemeyer and D. Vidovic, *Inorg. Chem.*, 2003, **42**, 4970–4976; (*j*) H. Zhou, E. J. Campbell and S. T. Nguyen, *Org. Lett.*, 2001, **14**, 2229–2231.

7 (*a*) C. Bour, J. Monot, S. Tang, R. Guillot, J. Farjon and V. Gandon, *Organometallics*, 2014, **33**, 594–599; (*b*) A. El-Hellani, J. Monot, S. Tang, R. Guillot, C. Bour and V. Gandon, *Inorg. Chem.*, 2013, **52**, 11493–11502; (*c*) A. Higelin, S. Keller, C. Göhringer, C. Jones and I. Krossing, *Angew. Chem., Int. Ed.*, 2013, **52**, 4941–4944; (*d*) A. El-Hellani, J. Monot, R. Guillot, C. Bour and V. Gandon, *Inorg. Chem.*, 2013, **52**, 506–514; (*e*) S. Tang, J. Monot, A. El-Hellani, B. Michelet, R. Guillot, C. Bour and V. Gandon, *Chem. – Eur. J.*, 2012, **18**, 10239–10243; (*f*) G. E. Ball, M. L. Cole and A. I. McKay, *Dalton Trans.*, 2012, **41**, 946–952; (*g*) S. G. Alexander, M. L. Cole and C. M. Forsyth, *Chem. – Eur. J.*, 2009, **15**, 9201–9214; (*h*) S. G. Alexander, M. L. Cole, S. K. Furfari and M. Kloth, *Dalton Trans.*, 2009, **16**, 2909–2911; (*i*) M. L. Cole, S. K. Furfari and M. Kloth, *J. Organomet. Chem.*, 2009, **694**, 2934–2940; (*j*) N. Marion, E. C. Escudero-Adán, J. Benet-Buchholz, E. D. Stevens, L. Fensterbank, M. Malacria and S. P. Nolan, *Organometallics*, 2007, **26**, 3256–3259; (*k*) C. Jones, D. P. Mills and R. P. Rose, *J. Organomet. Chem.*, 2006, **691**, 3060–3064; (*l*) R. J. Baker, H. Bettentrup and C. Jones, *Eur. J. Inorg. Chem.*, 2003, **13**, 2446–2451; (*m*) R. J. Baker and C. Jones, *Appl. Organomet. Chem.*, 2003, **17**, 807–808; (*n*) R. J. Baker, R. D. Farley, C. Jones, M. Kloth and D. M. Murphy, *Chem. Commun.*, 2002, **11**, 1196–1197; (*o*) R. J. Baker, M. L. Cole, C. Jones and M. F. Mahon, *Dalton Trans.*, 2002, **9**, 1992–1996; (*p*) R. J. Baker, A. J. Davies, C. Jones and M. Kloth, *J. Organomet. Chem.*, 2002, **656**, 203–210; (*q*) C. D. Abernethy, M. L. Cole and C. Jones, *Organometallics*, 2000, **19**, 4852–4857; (*r*) M. D. Francis, D. E. Hibbs, M. B. Hursthouse, C. Jones and N. A. Smithies, *Dalton Trans.*, 1998, **19**, 3249–3254; (*s*) D. E. Hibbs, M. B. Hursthouse, C. Jones and N. A. Smithies, *Chem. Commun.*, 1998, **8**, 869–870; (*t*) S. J. Black, D. E. Hibbs, M. B. Hursthouse, C. Jones, K. M. A. Malik and N. A. Smithies, *Dalton Trans.*, 1997, **22**, 4313–4319.

8 Rohm and Hass Electronic Materials LLC, Synthesis of trimethylgallium, *U.S. Patent* 2006/47132A1, 2006.

9 I. Pérez, J. P. Sestelo and L. A. Sarandeses, *J. Am. Chem. Soc.*, 2001, **123**, 4155–4160.

10 Horeglad *et al.* previously reported the obtention of complexes **1** and **2** *via* an indirect synthetic route,[4a,b] in which the reaction of 2 equivalents of a NHC alkoxy dimethyl-gallium complex with an equal amount of GaMe$_3$ yielded complexes IMes·GaMe$_3$ (**G**) and SIMes·GaMe$_3$ (**J**) and a dimeric dialkylgallium byproduct. As for complex **4**, it has been recently reported according to Scheme 1 to yield SIPrGaMe$_3$ (**I**) and the structure was used to compare the coordination properties of **G**[3c] and **J**[3e] with respect to their reactivity in the polymerization of *rac*-LA.[3c] Nevertheless, these complexes have been included in this report to maintain the rigor of our studies.

11 A. M. Magill, K. J. Cavell and B. F. Yates, *J. Am. Chem. Soc.*, 2004, **126**, 8717–8724.

12 H. V. Huynh, Y. Han, R. Jothibasu and J. A. Yang, *Organometallics*, 2009, **28**, 5395–5404.

13 S. Leuthäußer, D. Schwarz and H. Plenio, *Chem. – Eur. J.*, 2007, **13**, 7195–7203.

14 G. Davidson, in *Characteristic Vibrations of Compounds of Main Group Elements*, ed. G. Davidson, Royal Society of Chemistry, UK, 2001, vol. 24, pp. 217–267.

15 (*a*) S. J. Ryan, S. D. Schimler, D. C. Bland and M. S. Sanford, *Org. Lett.*, 2015, **17**, 1866–1869; (*b*) X. Bantreil and S. P. Nolan, *Nat. Protoc.*, 2011, **6**, 69–77; (*c*) M. K. Denk, J. M. Rodezno, S. Gupta and A. J. Lough, *J. Organomet. Chem.*, 2001, **617–618**, 242–253; (*d*) A. J. Arduengo, R. Krafczyk and R. Schmutzler, *Tetrahedron*, 1999, **55**, 14523–11453.

16 (*a*) H. Clavier and S. P. Nolan, *Chem. Commun.*, 2010, **46**, 841–861; (*b*) A. Poater, B. Cosenza, A. Correa, S. Giudice, F. Ragone, V. Scarano and L. Cavallo, *Eur. J. Inorg. Chem.*, 2009, **13**, 1759–1766.

17 H. Jacobsen, A. Correa, A. Poater, C. Costabile and L. Cavallo, *Coord. Chem. Rev.*, 2009, **253**, 687–703.

18 (*a*) N. Holzmann, A. Stasch, C. Jones and G. Frenking, *Chem. – Eur. J.*, 2013, **19**, 6467–6479; (*b*) N. Holzmann, A. Stasch, C. Jones and G. Frenking, *Chem. – Eur. J.*, 2011, **17**, 13517–13525.

19 L. Falivene, L. Caporaso, L. Cavallo and H. Jacobsen, *Dalton Trans.*, 2013, **42**, 7281–7286.

20 *SMART version 5.628*, Bruker AXS Inc., Madison, WI, USA, 2001.

21 G. M. Sheldrick, *SADABS V2014/4 (Bruker AXS Inc.)*, University of Göttingen, Göttingen, Germany, 2014.

22 *SHELXTL-2014/6 (Sheldrick, 2014)*, Bruker AXS Inc., Madison, WI, USA, 2014.

23 E. J. Baerends, D. E. Ellis and P. Ros, *Chem. Phys.*, 1973, **2**, 41–51.

24 L. Versluis and T. Ziegler, *J. Chem. Phys.*, 1988, **88**, 322–328.

25 (*a*) G. te Velde, F. M. Bickelhaupt, E. J. Baerends, C. F. Guerra, S. J. A. van Gisbergen, J. G. Snijders and T. Ziegler, *J. Comput. Chem.*, 2001, **22**, 932–942; (*b*) C. F. Guerra, J. G. Snijders, G. te Velde and E. J. Baerends, *Theor. Chem. Acc.*, 1998, **99**, 391–403; (*c*) E. J. Baerends, *et al.*, *SCM, Theoretical Chemistry*, Vrije Universiteit, Amsterdam, The Netherlands, http://www.scm.com; ADF2008-01.

26 J. C. Slater, *Phys. Rev.*, 1951, **81**, 385–390.

27 S. H. Vosko, L. Wilk and M. Nusair, *Can. J. Phys.*, 1980, **58**, 1200–1211.

28 A. D. Becke, *Phys. Rev. A*, 1988, **38**, 3098–3100.

29 J. P. Perdew, *Phys. Rev. B: Condens. Matter*, 1986, **33**, 8822–8827.

30 E. van Lenthe and E. J. Baerends, *J. Comput. Chem.*, 2003, **24**, 1142–1156.